ADVANCED MATERIALS

www.advmat.de

Phthalocyanine–Virus Nanofibers as Heterogeneous Catalysts for Continuous-Flow Photo-Oxidation Processes

Eduardo Anaya-Plaza, Ana Aljarilla, Grégory Beaune, Nonappa, Jaakko V. I. Timonen, Andrés de la Escosura, Tomás Torres, and Mauri A. Kostiainen**

The generation of highly reactive oxygen species (ROS) at room temperature for application in organic synthesis and wastewater treatment represents a great challenge of the current chemical industry. In fact, the development of biodegradable scaffolds to support ROS-generating active sites is an important prerequisite for the production of environmentally benign catalysts. Herein, the electrostatic cocrystallization of a cationic phthalocyanine (Pc) and negatively charged tobacco mosaic virus (TMV) is described, together with the capacity of the resulting crystals to photogenerate ROS. To this end, a novel peripherally crowded zinc Pc (1) is synthesized. With 16 positive charges, this photosensitizer shows no aqueous aggregation, and is able to act as a molecular glue in the unidimensional assembly of TMV. A step-wise decrease of ionic strength in mixtures of both components results in exceptionally long fibers, constituted by hexagonally bundled viruses thoroughly characterized by electron and confocal microscopy. The fibers are able to produce ROS in a proof-of-concept microfluidic device, where they are immobilized and irradiated in several cycles, showing a resilient performance. The bottom-up approach also enables the light-triggered disassembly of fibers after use. This work represents an important example of a biohybrid material with projected application in light-mediated heterogeneous catalysis.

Dr. E. Anaya-Plaza, Dr. Nonappa, Prof. M. A. Kostiainen
Department of Bioproducts and Biosystems
Aalto University
Kemistintie 1, 02150 Espoo, Finland
E-mail: mauri.kostiainen@aalto.fi

Dr. A. Aljarilla, Dr. A. de la Escosura, Prof. T. Torres
Department of Organic Chemistry
Universidad Autónoma de Madrid (UAM)
Calle Francisco Tomás y Valiente, 7, 28049 Madrid, Spain
E-mail: tomas.torres@uam.es

Dr. G. Beaune, Dr. Nonappa, Prof. J. V. I. Timonen
Department of Applied Physics
Aalto University School of Science
Puumiehenkuja 2, FI-02150 Espoo, Finland

Dr. A. de la Escosura, Prof. T. Torres
Institute for Advanced Research in Chemical Sciences (IAdChem)
UAM
Campus de Cantoblanco, 28049 Madrid, Spain

Prof. T. Torres
IMDEA-Nanociencia
Campus de Cantoblanco, 28049 Madrid, Spain

The ORCID identification number(s) for the author(s) of this article can be found under https://doi.org/10.1002/adma.201902582.

DOI: 10.1002/adma.201902582

Visible-light-mediated oxidation is a fast-developing field with applications in organic synthesis[1] and wastewater treatment.[2,3] In particular, molecular oxygen as oxidation source has gained focused attention, as it is considered as an environmental-friendly approach.[4] In this direction, organic chromophores such as porphyrinoids have been employed to convert nonreactive O_2 into reactive oxygen species (ROS) at room temperature, with wide application in nanomedicine[5,6] and catalysis.[7] Dye-containing heterogeneous catalysts can be easily separated from the reaction medium, offering advantages for scale-up and continuous-flow processes. Highly ordered structures, such as metal–organic frameworks, have been exploited in this direction as scaffolds to support photoactive molecules in a biomimetic approach.[7,8] However, even if the photo-oxidation process itself is as environmentally friendly as possible, a major drawback of these catalysts active sites or structural scaffolds rely on heavy metal atoms.[9–11] These undesirable components represent an environmental hazard and, therefore, development of biodegradable supported catalysts is of paramount importance.

Proteins are one of the most functional and versatile biomacromolecules employed by nature in molecular recognition, transport, and catalysis. Creating highly ordered structures via bottom-up assembly of proteins and designed synthetic materials, can lead to fascinating functional biohybrids that combine the best features of biological and synthetic matter.[12,13] Among all the chemical assembly strategies employed,[14,15] electrostatic interactions present important advantages. For example, they enable the use of native proteins without genetic or chemical modification and offer the possibility to design multistimuli assembly/disassembly processes, capital in the design of responsive materials.[16,17] The role that shape,[18] electrostatic potential,[19–21] and specific nearest neighbor interactions of the protein scaffold plays in the crystallization process is well-established.[22,23] Importantly, strategies to control the interaction between the protein and the cocrystallization agent by means of pH and ionic strength of the aqueous media has enabled fine tuning in the kinetics of the assembly process, leading to high structural control. Recent examples of protein crystal scaffolds with catalytic activity indicate that biohybrids can function

as efficient catalysts.[24–27] While protein cages such as (apo) ferritin or cowpea chlorotic mottle virus have coped the most recent developments in 3D electrostatic assemblies, other protein scaffolds such as tobacco mosaic virus (TMV) have been recently explored, yielding unidimensional morphologies.[28]

Among the porphyrinoids available, phthalocyanines (Pc) hold a prominent place due to their outstanding optical properties.[29–31] These non-natural photosensitizers consist of four isoindole units linked through nitrogen atoms, which are extendedly conjugated and yield intense absorption in the red/near-infrared region of the visible spectrum. In particular, zinc derivatives (ZnPc) present a characteristic sharp absorption band between 670–700 nm, as well as moderate to high fluorescence quantum yields. Furthermore, ZnPc are reported to produce ROS, a compendium of highly reactive oxidation agents such as superoxide, peroxides, and singlet oxygen, which can be utilized in photodynamic therapy, diagnostic arrays, and catalysis. We have previously reported spherical protein cage-Pc cocrystal with maintained light-induced excited state properties.[32] Herein, we report the enhanced properties arising from the cocrystallization between rod-like TMV and a highly charged ZnPc via electrostatic interactions into highly ordered fibers. Immobilization of the dye in fibers, in comparison with the dye free in solution, yields a heterogeneous catalyst allowing rapid purification by physical methods. Additionally, the high aspect ratio of the fibers gives a high contact area with the media. On the other hand, the use of responsive self-assembled biohybrids allows us to dispose them with the adequate stimuli, yielding exclusively biodegradable material. Such assemblies can be used as aqueous media oxidizing agents with potential application in green organic chemistry and water treatment.

The use of Pc in aqueous media is associated with several challenges, such as lack of solubility, high hydrophobicity, and aggregation, compromising their performance. In order to circumvent these issues, we have designed and synthesized a novel ZnPc bearing eight 2,6-bis-(3-methylpyridinium) phenyloxy moieties (**1**) at the β position of the isoindole units (**Figure 1**a). The challenging synthesis of this unique chromophore was accomplished in four main steps (Scheme S1, Supporting Information). Briefly, 2-benzyloxy-1,3-dibromobenzene was coupled with pyridin-3-ylboronic acid via Suzuki–Miyaura reaction which, after deprotection, yielded 2,6-(bis(pyridine-3-yl))phenol. Second, nucleophilic aromatic substitution of 4,5-dichlorophthalonitrile with the previously synthesized phenol led to the desired disubstituted phthalonitrile exclusively under highly energetic microwave radiation. Otherwise, thermal reaction in the same conditions yielded the monosubstituted derivative due to the high steric hindrance of the nucleophilic groups. The third step consisted on the cyclotetramerization of the described phthalonitrile in the presence of $Zn(OAc)_2$, resulting into the precursor phthalocyanine bearing 16 pyridine groups (compound **8** in the Supporting Information). Last, permethylation of **8** in presence of methyl iodide resulted in the water soluble ZnPc **1**. The substitution pattern in this molecule renders a unique photosensitizer with enhanced performance in aqueous media. Peripheral decoration directs the 16 positively charged moieties out of the ZnPc plane (Figure 1b), hindering the typical columnar aggregation through π–π stacking in aqueous environment, which is

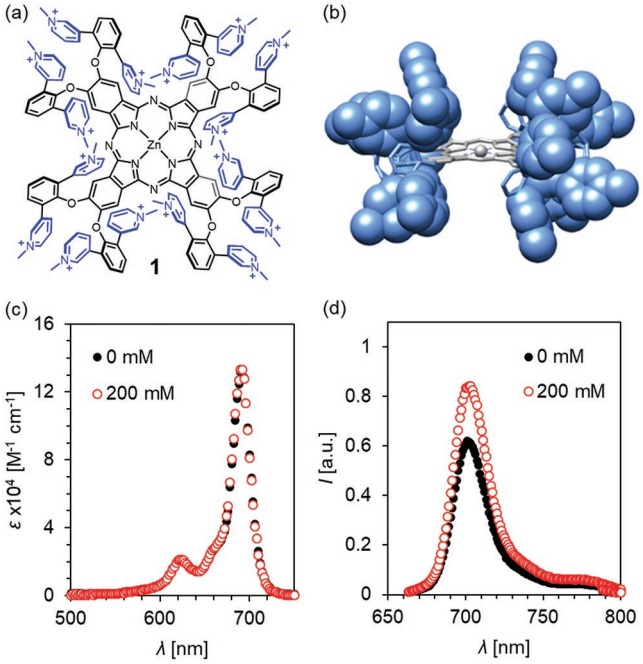

Figure 1. a) Chemical structure of ZnPc **1**. Iodide counterions are omitted for clarity. b) 3D structure obtained by ab initio calculations at semiempirical level (PM3). Pyridinium moieties shown as spheres. c) Absorption and d) emission spectra of **1** at 0 and 200×10^{-3} M of NaCl.

known to quench excited-state properties such as fluorescence and ROS production. This was clearly shown by the sharp absorption band observed in a broad range of salt concentrations (Figure 1c), as well as maintained emission when excited at 615 nm (Figure 1d). On the other hand, other water soluble ZnPc bearing eight *N*-methylpyridinium moieties (compound **9** in the Supporting Information) presented a strong aggregation by increasing NaCl concentration, as shown by the band shift from 675 to 635 nm as well as a complete emission quench (Figure S1, Supporting Information).

TMV is a helical array of 2130 coat proteins of an approximate molecular weight of 17 kDa, wrapping the viral RNA. This results in a 300 nm long, 18 nm diameter rod-like virus with an estimate molecular weight of 39.4 MDa (**Figure 2**a,b). This geometry, which renders a negatively charged helix on the outer surface of the virus at pH above 4.5,[33] can function as a well-defined scaffold for unidimensional ensembles. TMV has been employed as drug delivery platform,[34–36] as well as building block in different biohybrid arrays together with small functional molecules,[37] or nanoparticles.[28,38,39]

In order to understand how **1** and TMV interact, the saturation ratio (i.e., full coverage of TMV by photosensitizers) between **1** and TMV was determined by dynamic light scattering (DLS). TMV concentration was fixed at 0.1 mg mL^{-1} and, assuming a molecular weight of 39.4 MDa, increasing ratios between 0 and 25 000 equivalents of **1** were added. We observed the decrease of the peak at 300 nm, which corresponds to the unimeric TMV, while a new peak above 2000 nm arises, which corresponds to aggregated TMV (Figure 2c). Monitoring the derived count rate, we found the initial increase of the signal above 1000 equivalents, establishing the starting point of

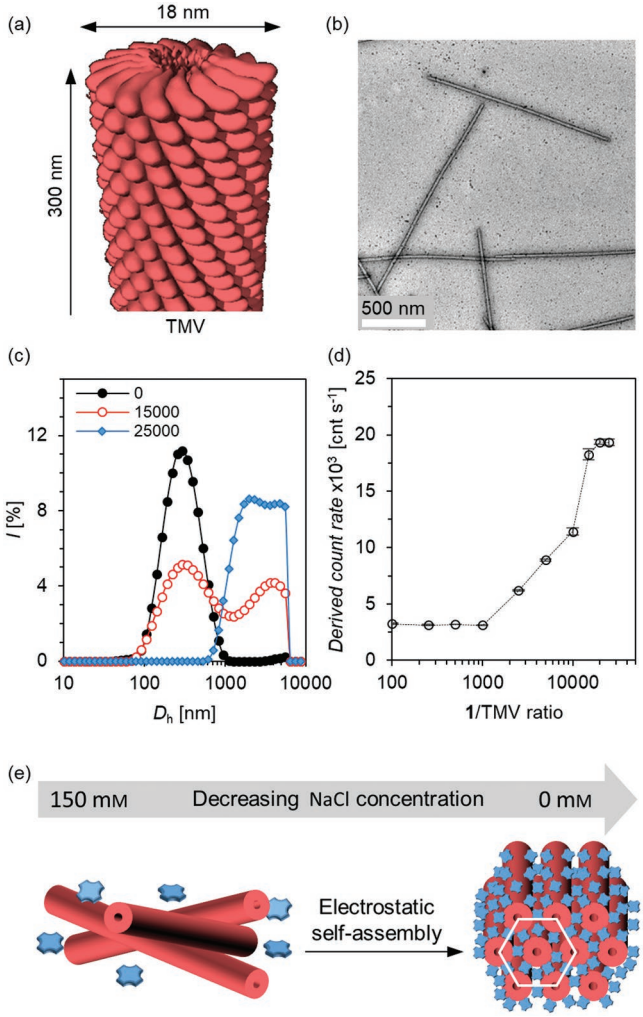

Figure 2. a) Structure model and b) TEM image of TMV. c) DLS intensity profiles of TMV (0.1 mg mL^{-1}) in presence of 0, 15 000, and 25 000 equivalents of **1** (black, red, and blue dots, respectively). d) Derived count rate of TMV (0.1 mg mL^{-1}) in presence of increasing ratios of **1**, showing saturation above 15 000 equivalents. e) Schematic representation of the step-wise approach to obtain crystalline hybrids, showing no interaction at high ionic strength (150×10^{-3} M NaCl) and high-ordered materials at low ionic strength (0×10^{-3} M NaCl).

assembly, while the saturation point was reached above 15 000 equivalents (Figure 2d). However, previously reported assembly of TMV shows concentration dependence.[40,41] In fact, when the concentration of the virus has risen to 10 mg mL^{-1}, saturation of the virus is reached above 10 000 equivalents, as we observe the precipitate formation, while a deep-colored supernatant remains. Therefore, unless stated otherwise, a ratio of 10 000 was employed in the following experiments.

Electrostatically assembled protein crystals are highly dependent on the ionic strength of the media. Therefore, preparation of high aspect-ratio fibers was achieved by step-wise decrease of the NaCl concentration in the media (Figure 2e). TMV and **1** were mixed in acetate buffer 10×10^{-3} M pH 5.5 containing 150×10^{-3} M of NaCl and no complex formation was observed. The solution was dialyzed against the same buffer containing 125×10^{-3}, 100×10^{-3}, 75×10^{-3}, 50×10^{-3}, 25×10^{-3}, and finally 0×10^{-3} M of NaCl, yielding the aforementioned fibers. This electrostatically driven assembly is fully reversible and the fibers show disassembly upon increasing the ionic strength (Figure S2, Supporting Information).

The resulting complexes were structurally characterized by different techniques (**Figure 3**). Optical microscopy images show the fibrous morphology of the bundles, with thread lengths in the hundreds of micrometers and thicknesses between 1–2 µm (Figure 3a). Taking into account the TMV dimensions (300 × 18 nm), this morphology is the consequence of a spontaneous highly directional assembly process, where TMV acts as self-assembling building block, providing a protein-based scaffold that supports the photosensitizer. Small angle X-ray scattering (SAXS, Figure 3b) measurements reveal that the fibers present 2D hexagonal packing perpendicular to the fiber vector. Three main diffraction peaks (q = 0.0354, 0.0632, and 0.0727 Å^{-1}) were found, which correspond to the reflections from (10), (11), and (20) planes, respectively. Linear fitting of the squared diffraction peak indices as a function of the measured q-values yields a lattice constant of a = 20.1 nm (Figure 3c). This is in good agreement with the typical packing of highly concentrated TMV,[42] or in presence of atomic cations[41,43] or small-size AuNPs.[28] The observed lattice parameter is slightly higher than the TMV diameter (i.e., 18 nm), which is in close agreement with the proposed model. On the other hand, direct combination of **1** and TMV capsids in acetate buffer 10×10^{-3} M pH 5.5 in the absence of NaCl results in the immediate sedimentation of a green-colored fibrous complex. Observed under the optical microscope, the fibers are shorter and thicker (Figure S3, Supporting Information). These quickly assembled fibers do not show any scattering peaks in SAXS analysis because of their amorphous structure.

Further structural insight of the highly ordered fibers was obtained by ambient- and cryo-electron microscopy (Figure 3d–f). High-magnification images of the fibers confirm the parallel alignment and side-by-side packing of the individual viruses. No periodic order along the fiber axis was observed, which supports the 2D structure obtained by SAXS. Additionally, cryo-TEM (transmission electron microscopy) images show similar features as observed in the macroscale, such as twists and bifurcations (Figure 3f). The helical twists were 3D reconstructed, showing a transfer of the chirality from the individual virus to the bundle. As shown in Figure 3g, right-handed helicity was found, which is in good agreement with previously reported TMV bundles.

As a consequence of the anisotropy inherent to 1D ordered materials, the fibers present birefringence of polarized light (**Figure 4**a). They show strong blue color when oriented 45° respect the crosspolarizers, in opposition to other possible orientations (Figure S4, Supporting Information). Otherwise, the interaction with the virus does not affect the optical properties of **1**, as shown by the sharp absorption of the hybrid at 692 nm (Figure 4b). This confirms the unaltered excited state properties of **1** even when packed with TMV. In fact, strong fluorescence of the fibers can be observed when irradiated at 633 nm. This property opens up new characterization possibilities like confocal microscopy, which offers better resolution than optical microscopy. Hybrids shown in Figure 4c were characterized with this technique and the images reinforce the hypothesis of the hierarchical fiber ensemble of smaller threads.

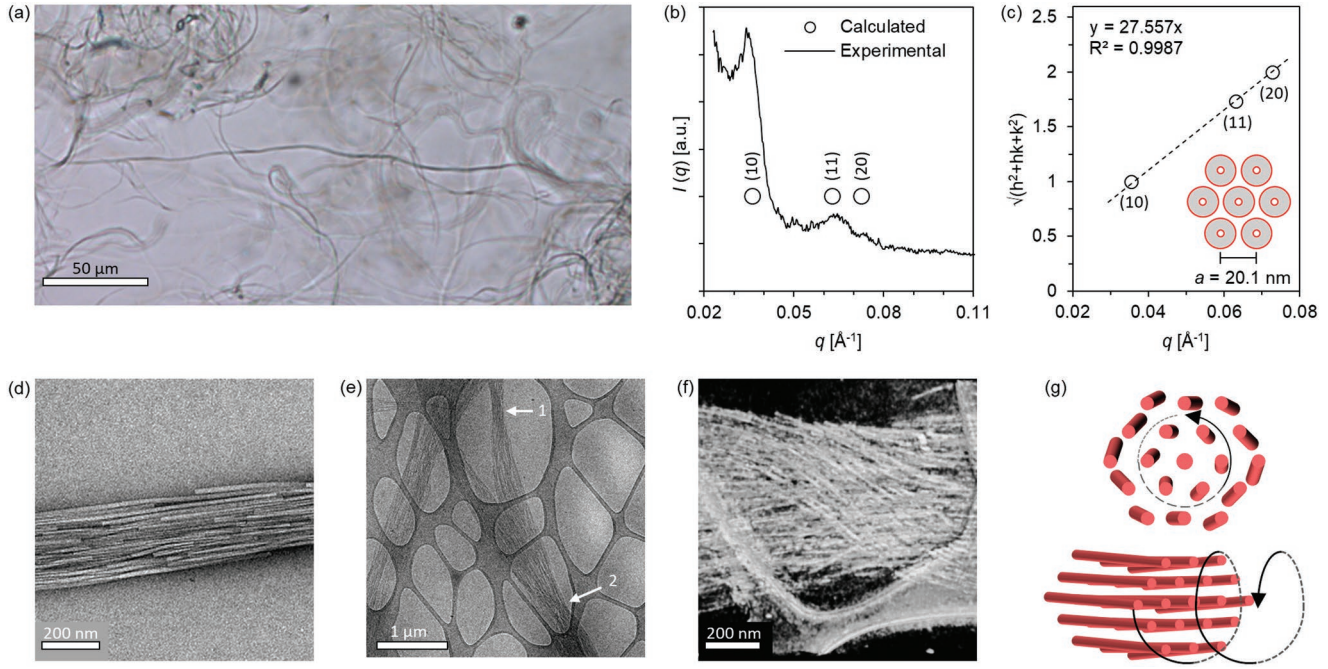

Figure 3. Structural characterization of the **1**-TMV fibers. a) Optical microscopy image showing the fibers and their entanglement. b) SAXS measured (line) of the hybrids. The simulated data (dots) were calculated assuming $a = 20.1$ nm. c) The squared diffraction peak indices plotted as a function of the measured q-values. A linear fit yields $a = 18.5$ nm for a 2D hexagonal lattice. d) TEM image showing the **1**-TMV fibers and e) their fine structure, constituted by parallel alignment of individual TMV capsids. f) Cryo-EM image of the biohybrids, showing features of their higher order organization in: 1) twists and 2) bundles to form bigger fibers. g) A cryo-ET density map of a twist, showing right-handed helicity.

Utilizing compound **1** as a molecular glue in the aforementioned biohybrids present several advantages, such as high solvent-accessible surface, which yields an ideal platform for heterogeneous photo-oxidation. In our approach, we hypothesize that **1** maintains its ROS generation ability despite the fact that it is immobilized within the biohybrid. In order to demonstrate this, ROS photogeneration was monitored by the well-known fluorescence indicator 2′,7′-dichlorodihydrofluorescein (H_2DCF) which oxidizes in presence of ROS to highly fluorescent 2′,7′-dichlorofluorescein (DCF, **Figure 5**a). The fibers were placed on a glass slide, covered with 750×10^{-6} M H_2DCF and then irradiated by excitation at 488 nm (green) and 633 nm (red). The former excites the sensor, while the latter excites the **1**-TMV fibers. Images were taken in a continuous way (each being the average of four images, 1.96 s per frame). We observed the DCF intensity increasing over the time exclusively in the near proximity of the fiber bundles (Figure 5b), as a consequence of the ROS photogeneration. On the other hand, areas without fibers present no emission in neither wavelength, serving as a negative control. Photo-oxidation dependence on molecular oxygen present in the media as well as the ZnPc was demonstrated in control experiments (Figures S5 and S6, Supporting Information).

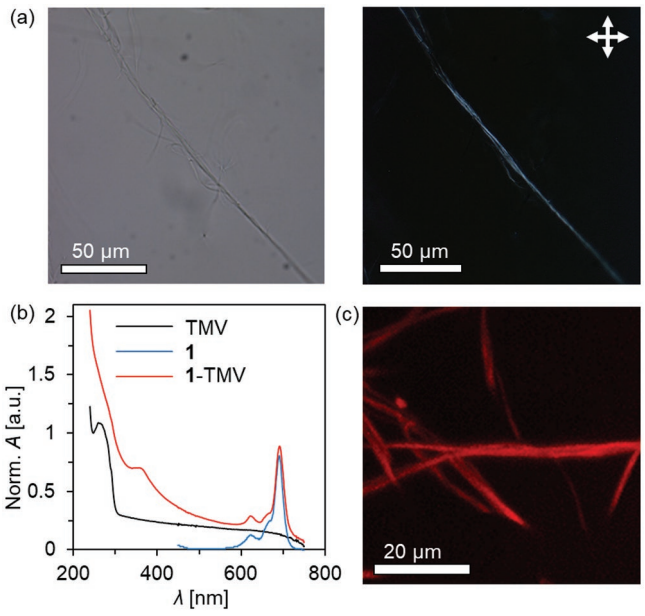

Figure 4. a) Optical (left) and polarized light (right) microscopy images. The latter was taken between crosspolarizers, aligned as shown in top-right corner vectors. b) Normalized absorption spectra of the **1**-TMV hybrid (red), compared to the TMV (black) and **1** (blue) in acetate buffer (10×10^{-3} M pH = 5.5). c) Confocal microscopy image of the hybrids ($\lambda_{exc} = 633$ nm).

One challenge of photochemical oxidation in aqueous media is to transfer this potential into continuous flow setups. However, our fiber-like morphology allowed to immobilize the bundles inside a proof-of-concept device (Figure S7, Supporting Information) consisting of a rectangular cross-section capillary ($0.2 \times 2.0 \times 50$ mm). The capillary was fed with H_2DCF 750×10^{-6} M in acetate buffer (10×10^{-3} M pH = 5.5), in order to maintain the conditions as close as possible to the formation of the fibers. Controlling the inlet flow and irradiation conditions allowed us to test the reproducibility of the ROS

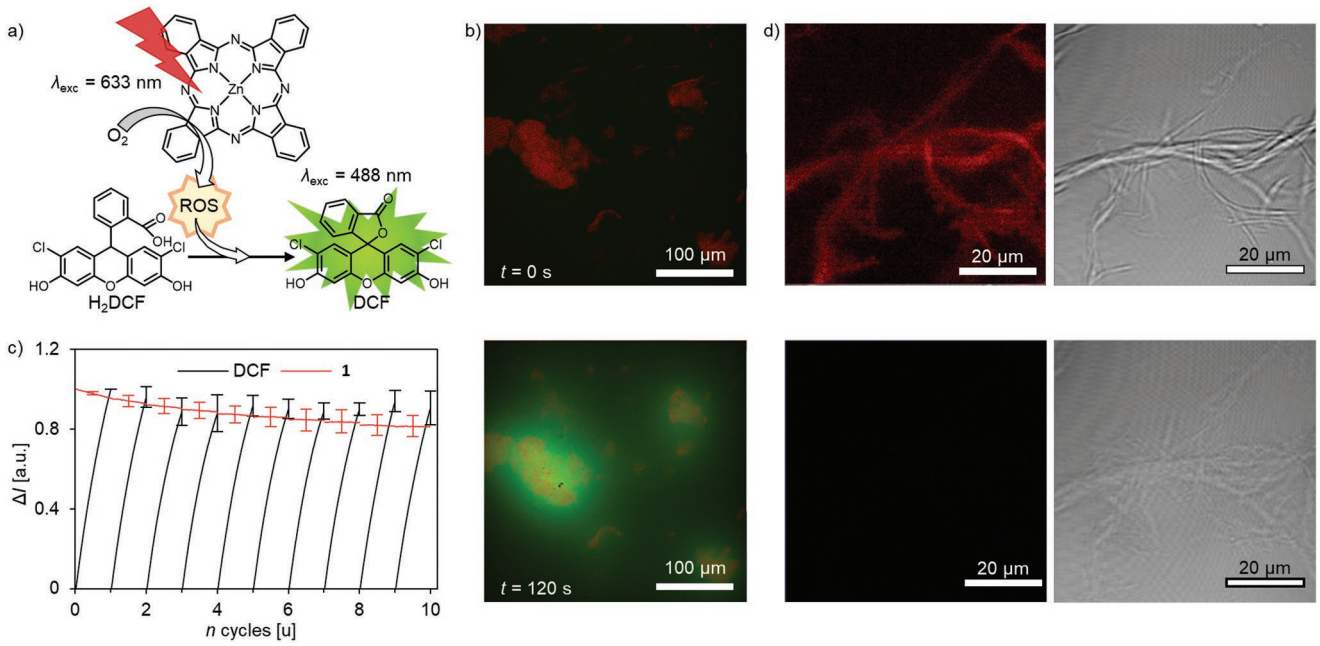

Figure 5. a) Schematic representation of the photoinduced oxidation process. Absorption of red light (λ_{exc} = 633 nm) by the chromophore induces the excitation of molecular oxygen present in the media to ROS, which oxidizes the precursor (H_2DCF, nonfluorescent) into DCF (λ_{exc} = 488 nm). Note that the peripheral substituents of **1** have been omitted for clarity purposes. b) Time-lapse emission microscopy images of the bundled fibers (red) and in situ photo-oxidized DCF (green). H_2DCF is present at 750×10^{-6} M in acetate buffer (10×10^{-3} M pH = 5.5). c) Averaged and normalized increase of DCF (black) and decrease of **1** (red) after 2 min irradiation (60 frames) per cycle. The error bars correspond to the standard deviation of three bundles. Normalized data to the end value of the first cycle (DCF) and the initial emission **1**. d) Emission (left) and bright field (right) microscopy images of fibers before (top) and after (bottom) intense irradiation, showing the photobleaching of the ZnPc and, as consequence, loss of their structural stability.

photogeneration and stability of the fibers under irradiation. In this setup, previously described irradiation conditions were employed, obtaining similar results after 2 min of continuous irradiation. Fluorescence intensity of DCF (green channel) was measured as the average of three circular ROI within the bundle and corrected with the average of three circular ROI far from the bundle, which serves as background signal. In a similar way, emission intensity of **1** was measured employing the same ROI in order to measure the fiber photostability. Subsequent washing with fresh H_2DCF solution (≈6 µL s^{-1} over 15 s) washed-out the remaining DCF without detaching the fibers, allowing us to repeat over 10 cycles. The average obtained from three bundles was plotted (Figure 5c). First, we observed remarkable stability of the fibers to the process: red intensity decreases just above 10% after 10 cycles (20 min of continuous irradiation). Additionally, no important intensity loss is observed between cycles, which support the effective immobilization of the fibers into the channel. Second, ROS production is consistent and stable, with a slight decrease in the final intensity due to the slight loss of photosensitizer.

One of the main advantages of supramolecularly assembled materials is their ability to disassemble under given stimuli. In our case, there is an opportunity to dispose the active material once the desired photo-oxidation has been achieved. To this end, the fibers were irradiated with laser intensities 20 times higher than the one used in the previous experiment. After a few seconds of irradiation, we observed a fast decrease in the emission as a consequence of the photobleaching of **1**, which triggers the dissolution of the samples as shown in the bright field images (Figure 5d). This results in a green solution to the disposal of the active materials, in opposition to the nonsoluble inorganic materials typically used in catalysis.

In conclusion, we have designed, synthesized, and characterized a new biohybrid material obtained by the electrostatic interaction between the TMV capsid and a specifically designed ZnPc, yielding a unique morphology with optical activity. The chromophore presents 16 positive charges and resilient optical properties in aqueous media of varying ionic strengths. The cationic chromophore can act as molecular glue and direct the assembly of the rod-like viruses into hexagonally packed fibers. Additionally to their interesting structural features, the resulting high aspect-ratio fibers maintain the optical properties of the dye, namely, fluorescence and singlet oxygen production. The first one allowed us to characterize the fibers by confocal microscopy. The second enabled us to demonstrate that the fibers are easily immobilized in capillaries, while their singlet oxygen production remains stable after several oxidation/flushing cycles. In addition, our self-assembly approach offers the possibility to disassemble the fibers by laser irradiation. This work represents a new approach to tackle continuous-flow photo-oxidation processes in aqueous media.

Supporting Information

Supporting Information is available from the Wiley Online Library or from the author.

Acknowledgements

E.A.-P. acknowledges the funding from the European Union's Horizon 2020 research and innovation programme under the Marie Sklodowska-Curie Grant Agreement No. 794536 (BiHyOMat). G.B. acknowledges the financial support of the Academy of Finland's Centers of Excellence Programme (HYBER). A.d.l.E. received support from the Spanish Ministry of Economy and Competitivity (MINECO: CTQ-2017-89539-P and EUIN2017-87022). T.T. acknowledges the financial support from the Spanish MINECO [CTQ2017-85393-P and PCIN-2017-042/EuroNanoMed2017-191, TEMPEAT]. IMDEA-Nanociencia acknowledges support from the "Severo Ochoa" program for Centres of Excellence in R&D (MINECO, Grant SEV-2016-0686). The support to M.A.K. by the Academy of Finland (Grants 308578 and 303804) and the Sigrid Juselius Foundation is gratefully acknowledged. This work made use of the Aalto University Nanomicroscopy Centre (Aalto NMC).

Conflict of Interest

The authors declare no conflict of interest.

Keywords

heterogeneous catalysis, phthalocyanines, reactive oxygen species, self-assembly, viral capsids

Received: April 23, 2019
Revised: June 10, 2019
Published online: August 8, 2019

[1] C. Bian, A. K. Singh, L. Niu, H. Yi, A. Lei, *Asian J. Org. Chem.* **2017**, *6*, 386.
[2] R. Ma, S. Zhang, T. Wen, P. Gu, L. Li, G. Zhao, F. Niu, Q. Huang, Z. Tang, X. Wang, *Catal. Today* **2018**, S0920586118315189.
[3] J. Herney-Ramirez, M. A. Vicente, L. M. Madeira, *Appl. Catal., B* **2010**, *98*, 10.
[4] S. Fukuzumi, Y.-M. Lee, J. Jung, W. Nam, *Green Chem.* **2018**, *20*, 948.
[5] V. Almeida-Marrero, E. van de Winckel, E. Anaya-Plaza, T. Torres, A. de la Escosura, *Chem. Soc. Rev.* **2018**, *47*, 7369.
[6] S. Singh, A. Aggarwal, N. V. S. D. K. Bhupathiraju, G. Arianna, K. Tiwari, C. M. Drain, *Chem. Rev.* **2015**, *115*, 10261.
[7] M. Zhao, S. Ou, C.-D. Wu, *Acc. Chem. Res.* **2014**, *47*, 1199.
[8] J. Chakraborty, I. Nath, F. Verpoort, *Coord. Chem. Rev.* **2016**, *326*, 135.
[9] Z. Lin, Z.-M. Zhang, Y.-S. Chen, W. Lin, *Angew. Chem., Int. Ed.* **2016**, *55*, 13739.
[10] C. Pereira, M. Simões, J. Tomé, F. Almeida Paz, *Molecules* **2016**, *21*, 1348.
[11] F. Scandola, C. Chiorboli, A. Prodi, E. Iengo, E. Alessio, *Coord. Chem. Rev.* **2006**, *250*, 1471.
[12] B. J. G. E. Pieters, M. B. van Eldijk, R. J. M. Nolte, J. Mecinović, *Chem. Soc. Rev.* **2016**, *45*, 24.
[13] S. Abe, B. Maity, T. Ueno, *Chem. Commun.* **2016**, *52*, 6496.
[14] Y. Bai, Q. Luo, J. Liu, *Chem. Soc. Rev.* **2016**, *45*, 2756.
[15] Q. Luo, C. Hou, Y. Bai, R. Wang, J. Liu, *Chem. Rev.* **2016**, *116*, 13571.
[16] M. A. Kostiainen, O. Kasyutich, J. J. L. M. Cornelissen, R. J. M. Nolte, *Nat. Chem.* **2010**, *2*, 394.
[17] V. Liljeström, J. Mikkilä, M. A. Kostiainen, *Nat. Commun.* **2014**, *5*, 4445.
[18] Y. Wang, Y. Wang, D. R. Breed, V. N. Manoharan, L. Feng, A. D. Hollingsworth, M. Weck, D. J. Pine, *Nature* **2012**, *491*, 51.
[19] A. M. Kalsin, M. Fialkowski, M. Paszewski, S. K. Smoukov, K. J. M. Bishop, B. A. Grzybowski, *Science* **2006**, *312*, 420.
[20] M. A. Kostiainen, P. Hiekkataipale, A. Laiho, V. Lemieux, J. Seitsonen, J. Ruokolainen, P. Ceci, *Nat. Nanotechnol.* **2013**, *8*, 52.
[21] A. H. Gröschel, A. Walther, T. I. Löbling, F. H. Schacher, H. Schmalz, A. H. E. Müller, *Nature* **2013**, *503*, 247.
[22] D. Nykypanchuk, M. M. Maye, D. van der Lelie, O. Gang, *Nature* **2008**, *451*, 549.
[23] S. Y. Park, A. K. R. Lytton-Jean, B. Lee, S. Weigand, G. C. Schatz, C. A. Mirkin, *Nature* **2008**, *451*, 553.
[24] M. Lach, M. Künzle, T. Beck, *Chem. - Eur. J.* **2017**, *23*, 17482.
[25] M. Künzle, T. Eckert, T. Beck, *J. Am. Chem. Soc.* **2016**, *138*, 12731.
[26] M. Uchida, K. McCoy, M. Fukuto, L. Yang, H. Yoshimura, H. M. Miettinen, B. LaFrance, D. P. Patterson, B. Schwarz, J. A. Karty, P. E. Prevelige, B. Lee, T. Douglas, *ACS Nano* **2018**, *12*, 942.
[27] N. K. Beyeh, Nonappa, V. Liljeström, J. Mikkilä, A. Korpi, D. Bochicchio, G. M. Pavan, O. Ikkala, R. H. A. Ras, M. A. Kostiainen, *ACS Nano* **2018**, *12*, 8029.
[28] V. Liljeström, A. Ora, J. Hassinen, H. T. Rekola, Nonappa, M. Heilala, V. Hynninen, J. J. Joensuu, R. H. A. Ras, P. Törmä, O. Ikkala, M. A. Kostiainen, *Nat. Commun.* **2017**, *8*, 671.
[29] H. Lu, N. Kobayashi, *Chem. Rev.* **2016**, *116*, 6184.
[30] A. B. Sorokin, *Chem. Rev.* **2013**, *113*, 8152.
[31] R. C. H. Wong, P.-C. Lo, D. K. P. Ng, *Coord. Chem. Rev.* **2019**, *379*, 30.
[32] J. Mikkilä, E. Anaya-Plaza, V. Liljeström, J. R. Caston, T. Torres, A. de la Escosura, M. A. Kostiainen, *ACS Nano* **2016**, *10*, 1565.
[33] M. Bendahmane, M. Koo, E. Karrer, R. N. Beachy, *J. Mol. Biol.* **1999**, *290*, 9.
[34] A. E. Czapar, Y.-R. Zheng, I. A. Riddell, S. Shukla, S. G. Awuah, S. J. Lippard, N. F. Steinmetz, *ACS Nano* **2016**, *10*, 4119.
[35] A. A. Vernekar, G. Berger, A. E. Czapar, F. A. Veliz, D. I. Wang, N. F. Steinmetz, S. J. Lippard, *J. Am. Chem. Soc.* **2018**, *140*, 4279.
[36] P. L. Chariou, L. Wang, C. Desai, J. Park, L. K. Robbins, H. A. Recum, R. A. Ghiladi, N. F. Steinmetz, *Macromol. Biosci.* **2019**, *19*, 1800407.
[37] Y. Tian, X. Yan, M. L. Saha, Z. Niu, P. J. Stang, *J. Am. Chem. Soc.* **2016**, *138*, 12033.
[38] E. Dujardin, C. Peet, G. Stubbs, J. N. Culver, S. Mann, *Nano Lett.* **2003**, *3*, 413.
[39] T. Nakajima, K. Sano, M. Mitsunaga, P. L. Choyke, H. Kobayashi, *Cancer Res.* **2012**, *72*, 4622.
[40] A. Nedoluzhko, T. Douglas, *J. Inorg. Biochem.* **2001**, *84*, 233.
[41] T. Li, R. E. Winans, B. Lee, *Langmuir* **2011**, *27*, 10929.
[42] T. Li, X. Zan, R. E. Winans, Q. Wang, B. Lee, *Angew. Chem., Int. Ed.* **2013**, *52*, 6638.
[43] L. Yang, S. Wang, M. Fukuto, A. Checco, Z. Niu, Q. Wang, *Soft Matter* **2009**, *5*, 4951.